HO_x budgets during HOxComp: A case study of HO_x chemistry under NO_x-limited conditions

Y. F. Elshorbany,[1,2,3] J. Kleffmann,[1] A. Hofzumahaus,[4] R. Kurtenbach,[1] P. Wiesen,[1] T. Brauers,[4] B. Bohn,[4] H.-P. Dorn,[4] H. Fuchs,[4] F. Holland,[4] F. Rohrer,[4] R. Tillmann,[4] R. Wegener,[4] A. Wahner,[4] Y. Kanaya,[5] A. Yoshino,[6,7] S. Nishida,[6,8] Y. Kajii,[6] M. Martinez,[9] D. Kubistin,[9] H. Harder,[9] J. Lelieveld,[9] T. Elste,[10] C. Plass-Dülmer,[10] G. Stange,[10] H. Berresheim,[11,12] and U. Schurath[13]

Received 13 October 2011; revised 20 December 2011; accepted 28 December 2011; published 10 February 2012.

[1] Recent studies have shown that measured OH under NO_x-limited, high-isoprene conditions are many times higher than modeled OH. In this study, a detailed analysis of the HO_x radical budgets under low-NO_x, rural conditions was performed employing a box model based on the Master Chemical Mechanism (MCMv3.2). The model results were compared with HO_x radical measurements performed during the international HOxComp campaign carried out in Jülich, Germany, during summer 2005. Two different air masses influenced the measurement site denoted as high-NO_x (NO, 1–3 ppbv) and low-NO_x (NO, < 1 ppbv) periods. Both modeled OH and HO_2 diurnal profiles lay within the measurement range of all HO_x measurement techniques, with correlation slopes between measured and modeled OH and HO_2 around unity. Recently discovered interference in HO_2 measurements caused by RO_2 cross sensitivity was found to cause a 30% increase in measured HO_2 during daytime on average. After correction of the measured HO_2 data, the model HO_2 is still in good agreement with the observations at high NO_x but overpredicts HO_2 by a factor of 1.3 to 1.8 at low NO_x. In addition, for two different set of measurements, a missing OH source of 3.6 ± 1.6 and 4.9 ± 2.2 ppb h^{-1} was estimated from the experimental OH budget during the low-NO_x period using the corrected HO_2 data. The measured diurnal profile of the HO_2/OH ratio, calculated using the corrected HO_2, is well reproduced by the MCM at high NO_x but is significantly overestimated at low NO_x. Thus, the cycling between OH and HO_2 is better described by the model at high NO_x than at low NO_x. Therefore, similar comprehensive field measurements accompanied by model studies are urgently needed to investigate HO_x recycling under low-NO_x conditions.

Citation: Elshorbany, Y. F., et al. (2012), HO_x budgets during HOxComp: A case study of HO_x chemistry under NO_x-limited conditions, *J. Geophys. Res.*, *117*, D03307, doi:10.1029/2011JD017008.

1. Introduction

[2] The hydroxyl radical (OH) has long been known as the primary oxidant in the atmosphere responsible for the oxidation and removal of most natural and anthropogenic trace gases. The major role of OH in the atmosphere was first recognized by *Levy* [1971]. Because of its short lifetime (<1 s), OH concentrations are determined by local chemical processes rather than transport. In addition, photochemical oxidation of volatile organic compounds (VOCs) results in

[1]Physikalische Chemie, Bergische Universität Wuppertal, Wuppertal, Germany.
[2]Environmental Research Division, National Research Centre, Cairo, Egypt.
[3]Now at Atmospheric Chemistry Department, Max-Plank Institute für Chemie, Mainz, Germany.
[4]Institut für Energie- und Klimaforschung, Forschungzentrum Jülich, Jülich, Germany.
[5]Research Institute for Global Change, Japan Agency for Marine-Earth Science and Technology, Yokohama, Japan.
[6]Department of Applied Chemistry, Tokyo Metropolitan University, Tokyo, Japan.
[7]Now at Environmental and Natural Resource Sciences, Tokyo University of Agriculture and Technology, Tokyo, Japan.
[8]Now at Environmental Renewable Energy System Division, Graduate School of Engineering, Gifu University, Gifu, Japan.
[9]Atmospheric Chemistry Department, Max-Plank Institute für Chemie, Mainz, Germany.
[10]Meteorologisches Observatorium, Deutscher Wetterdienst, Hohenpeissenberg, Germany.
[11]Meteorologisches Observatorium, Deutscher Wetterdienst, Hohenpeissenberg, Germany.
[12]Now at School of Physics and Centre for Climate and Air Pollution Studies, National University of Ireland Galway, Galway, Ireland.
[13]IMK-AAF, Karlsruhe Institute of Technology, Karlsruhe, Germany.

0148-0227/12/2011JD017008

the formation of other important radical intermediates, hydroperoxy (HO_2), organic peroxy (RO_2) and peroxyacyl (RCO_3) radicals. $\sum RO_2 + RCO_3$ are hereafter collectively referred to as RO_2. Since the OH radical controls the oxidation capacity of the atmosphere, the identification of its sources and sinks in the atmosphere is crucial for the understanding of the tropospheric chemistry under both polluted high NO_x as well as under low- NO_x conditions. The term "oxidation capacity" (OC) is defined in the current study as the sum of the respective oxidation rates of the molecules Y_i (VOCs, CO) by the oxidant X (X = OH, O_3, NO_3) [*Geyer et al.*, 2001]:

$$OC = \sum(k_{Y_i} \cdot [Y_i] \cdot [X]), \quad (1)$$

where k_{Yi} is the bimolecular rate constant for the reaction of Y_i with X (for the argument of using this definition, see *Elshorbany et al.* [2009a]).

[3] Two widely applied chemical schemes to investigate HO_x ($OH+HO_2$) chemistry are the Regional Atmospheric Chemistry Mechanism (RACM) [*Stockwell et al.*, 1997], which uses lumped reactions for organic compounds, and the Master Chemical Mechanism (MCM), a near-explicit chemical mechanism (http://mcm. leeds.ac.uk/MCM/). The MCM is based on the original protocol, MCMv2 devised by *Jenkin et al.* [1997], which has been updated and subsequently improved to MCMv3.0 [*Saunders et al.*, 2003; *Jenkin et al.*, 2003]. The aromatic degradation chemistry schemes within MCMv3.0 have been substantially updated, described in MCMv3.1 [*Bloss et al.*, 2005a, 2005b]. The most explicit version, MCMv3.2 incorporates the recent updates of isoprene chemistry [*Paulot et al.*, 2009a, 2009b; *Lockwood et al.*, 2010]. In addition to the more explicit mechanism of isoprene, OH recycling from the reaction of acyl peroxy radicals with HO_2 (based on the IUPAC recommendation for $CH_3C(O)O_2+HO_2$) has been newly implemented in MCMv3.2. In addition, specialized chemical mechanisms were developed for isoprene, such as the Mainz Isoprene Mechanism (MIM) [*Pöschl et al.*, 2000; *von Kuhlmann et al.*, 2004; *Sander et al.*, 2005] and its updated version MIM2 [*Taraborrelli et al.*, 2009] or the modified version MIM-GK [*Geiger et al.*, 2003; *Karl et al.*, 2006], which can be used alone or in conjunction with other chemical schemes especially for isoprene-rich environments [e.g., *Lelieveld et al.*, 2008; *Hofzumahaus et al.*, 2009; *Pugh et al.*, 2010].

[4] In general, field studies of HO_x in rural environments showed that OH levels were well simulated during high-NO_x events (e.g., BERLIOZ [*Mihelcic et al.*, 2003], TOHPE [*Mount and Williams*, 1997], TORCH [*Emmerson et al.*, 2007], and PRIDE-PRD2006 [*Hofzumahaus et al.*, 2009]). However, under low-NO_x conditions in isoprene-rich air, modeled OH levels tend to be underpredicted. For example, in a recent field campaign in the rural area of the Pearl River Delta (PRD), China, *Hofzumahaus et al.* [2009] found that modeled OH using a photochemical box model based on RACM updated with MIM-GK, underpredicted measured OH under low-NO_x conditions. This result was confirmed by measuring the sources and sinks of the OH radical. Thus, they proposed a missing OH source and suggested additional radical cycling (without NO) to fill this gap. Such significant underestimation of OH levels was previously reported over the pristine forests of Surinam, Guyana and the French Guyana using an atmospheric chemistry model based on MIM [*Lelieveld et al.*, 2008, and references therein]. Recently, a significant OH underestimation was also observed during the OP3 campaign performed at the top of the rain forest canopy near Danum Valley, Malaysian Borneo using a box model based mainly on MIM2 [*Pugh et al.*, 2010, and references therein] or MCM [*Whalley et al.*, 2011; *Stone et al.*, 2011].

[5] In summer 2005, a blind international HO_x intercomparison (HOxComp) was carried out at Forschungszentrum Jülich (FZJ), which is located in a mixed deciduous forest in a rural environment in Germany [*Schlosser et al.*, 2009; *Fuchs et al.*, 2010]. In addition to HO_x measurements, a large set of ancillary parameters including OH reactivity, oxygenated volatile organic compounds (OVOCs) and major OH radical precursors were measured during three days (9–11 July) of ambient air sampling. These measurements offer the unique opportunity to investigate the HO_x chemistry at rural conditions with variable NO_x levels, based on data from different HO_x instruments. Two model studies have been performed to analyze the field data. The present work is a case study of the HO_x budgets of a selected day (10 July), analyses the contributions of primary HO_x sources and recycling, and compares the measured HO_x concentrations with box model simulations based on most explicit chemical scheme MCMv3.2. *Kanaya et al.* [2011] extended the model measurement comparison to the other HOxComp days based on RACM with updated isoprene chemistry and investigated the impact of different, recently proposed isoprene mechanisms on the predicted HO_x concentrations.

2. Methodology

2.1. HOxComp Campaign

[6] Only a brief description of the campaign is given here. For more details, see *Schlosser et al.* [2009] and *Fuchs et al.* [2010]. The HOxComp campaign took place on the campus of FZJ (50°54′33″N, 06°24′44″E). The campus is situated in a mixed deciduous forest about 2–3 km southeast of the city of Jülich and is surrounded by agricultural areas and main roads. The formal part of the campaign included 3 days of ambient measurements (9–11 July 2005) and 6 days of chamber experiments in the SAPHIR chamber (17–23 July 2005), of which only ambient measurements will be compared to model simulations. During the weekend days 9–10 July 2005, essentially no traffic occurred on the campus [*Schlosser et al.*, 2009]. Of the 3 day ambient measurements, sunny and clear sky conditions were available only on 10 July. On 11 July, HO_x data were only available until about 14:00 UTC, when a rainstorm evolved and OH reactivity measurements were available only for about 1 h from 13:00 to 14:00 UTC, which causes the 11 July data to be unsuitable for the calculation of experimental HO_x budgets (see section 3.6). On 9 July, very high NO_x levels were observed during the daytime, leading to much lower HO_2 levels [*Fuchs et al.*, 2010]. Under these conditions, an average of 9–10 July would mask the low-NO_x conditions experienced by the measurement site on 10 July (see sections 3.3 and 3.4), which is the main focus of this study. In addition, model simulations of 9–11 July were performed using RACM-based box model [*Kanaya et al.*, 2011].

Therefore, only 10 July is considered here as case study for the simulation and analysis of the radical budgets.

2.2. Ambient Measurements

[7] Detailed analyses of the formal blind intercomparison of the different OH and HO_2 measurement techniques are published by *Schlosser et al.* [2009] and *Fuchs et al.* [2010], respectively. In short, OH measurements in ambient air were compared for four different instruments: three laser-induced fluorescence (LIF) instruments operated by Max-Planck Institute Mainz (MPI-LIF); Forschungszentrum Jülich (FZJ-LIF) and the Japan Frontier Research Centre for Global Change (FRCGC-LIF) and one chemical ionization mass spectrometry (CIMS) instrument operated by the Deutscher Wetterdienst (DWD-CIMS), each using its own calibration scheme. In SAPHIR, the OH measurements by the LIF instruments were compared to measured data from the Differential Optical Absorption Spectroscopy (DOAS) instrument operated by FZJ, without participation of the CIMS instrument. All LIF instruments additionally measured HO_2 through the chemical conversion to OH by addition of NO in the gas expansion, followed by LIF detection of the additionally formed OH. Total OH reactivity was measured by the laser-induced pump and probe technique; detailed description of the instrument is published elsewhere [*Yoshino et al.*, 2006, and references therein]. The uncertainty in the reactivity data during the HOxComp was estimated to be 15% [*Kanaya et al.*, 2011].

[8] In SAPHIR, OH measurements by the LIF and DOAS instruments showed very good agreement within 12%, well within the specified calibration errors. In ambient air, however, the regression between pairs of LIF instruments showed slopes between 1.06 (FZJ-LIF versus FRCGC-LIF) and 1.29 (MPI-LIF versus FZJ-LIF), while regressions between CIMS and LIF instruments had slopes between 0.59 (DWD-CIMS versus MPI-LIF) and 0.75 (DWD-CIMS versus FRCGC-LIF). The increased discrepancies in ambient air were possibly caused by inhomogeneously mixed air and/or possible changes of the OH measurement sensitivities that are not accounted for by calibration [*Schlosser et al.*, 2009].

[9] For the HO_2 measurements in SAPHIR, the three LIF instruments were found to agree within the combined 1σ calibration errors (about 30%), when the water vapor mixing ratio in SAPHIR was in the range of (0.6–1.8)% [*Fuchs et al.*, 2010]. Larger systematic deviations were found in dry air. Owing to the relatively high humidity in ambient air, good agreement would be expected, as in the SAPHIR experiments. In fact, the regression of the HO_2 data in ambient air yielded slopes of 1.19 for FRCGC-LIF versus FZJ-LIF, 0.59 for FZJ-LIF versus MPI-LIF and 1.46 for MPI-LIF versus FRCGC-LIF during daytime. The reason for the larger discrepancies compared to the SAPHIR experiments could not be resolved [*Fuchs et al.*, 2010]. One possible reason was discovered after HOxComp. Interference in HO_2 measurements by FZJ-LIF was detected which is caused by cross sensitivity to specific RO_2 radicals [*Fuchs et al.*, 2011]. The interference has been confirmed for the MPI-LIF instrument (T. Dillon (interactive comment, 2011) to *Fuchs et al.* [2011]), and was likely present also in the FRCGC-LIF instrument. The level of interference depends on specific instrumental parameters and may be different for each LIF instrument at HOxComp. So far, it has been characterized for FZJ-LIF only, showing relative sensitivities to RO_2 compared to HO_2 in the range of (50–95)% for peroxy radicals from alkenes, isoprene, MVK, MACR and aromatic compounds [*Fuchs et al.*, 2011]. The interference causes a systematic overprediction of the measured HO_2 concentrations depending on the specific air composition. A detailed description of the experimental setup of the interference experiment for the FZJ_LIF is given by *Fuchs et al.* [2011], which can be used as a guide to characterize the interferences in other LIF instruments.

[10] For the purpose of the comparison between measured and simulated HO_x concentrations, mean measured OH and HO_2 data by all instruments is used in the current study (see section 3.5). During daytime, the measurements by individual instruments fall into an interval of about ± 30% around their mean. This interval represents the experimental uncertainty of the observations due to systematic differences between the individual instruments. For HO_2, the interference contributes an additional systematic error, which is discussed in section 3.

[11] Measured trace gases included HONO, HCHO, NO, NO_2, CO, O_3, volatile organic compounds (VOCs) and photolysis frequencies $j(NO_2)$, $j(O^1D)$, j(HCHO), j(HONO). Meteorological parameters including temperature, pressure, relative humidity, wind speed and wind direction were also measured using standard techniques. The time in the current study is reported as UTC. Sunrise, local noon, and sunset occurred at 03:34, 11:40, and 19:45 UTC. Daytime is defined from 06:00 to 18:00 UTC.

2.3. Modeling Approach

[12] A zero-dimensional photochemical box model based on the Master Chemical Mechanism, MCMv3.2 (http://mcm.leeds.ac.uk/MCM) has been used to evaluate the radical budgets during HOxComp. The MCM photochemical box model system of simultaneous stiff ordinary differential equations (ODEs) was integrated with a variable order Gear's method (FACSIMILE [*Curtis and Sweetenham*, 1987]). The model was constrained by 10 min average values of the following measured parameters: $j(NO_2)$, $j(O^1D)$, j(HONO), $j(HCHO_{radical})$, relative humidity, pressure, temperature, NO, NO_2, HONO, CO, HCHO, O_3, and 27 hydrocarbons (including isoprene) and oxygenated VOCs (see section 3.1). The other photolysis frequencies are parameterized within the model using a two stream isotropic scattering model under clear sky conditions [*Hayman*, 1997; *Saunders et al.*, 2003]. The photolysis rates are calculated as a function of solar zenith angle and adjusted by a scaling factor, calculated from the ratio of measured and model calculated $j(NO_2)$ values, which takes into account the effects of varying cloud cover and aerosol scattering. Dry deposition terms have been incorporated in the model based on the values of *Sommariva et al.* [2006, and references therein] for HNO_3 (2 cm s^{-1}), NO_2 (0.15 cm s^{-1}), PAN (0.2 cm s^{-1} and assumed the same for the other PANs), O_3 (0.5 cm s^{-1}), SO_2 (0.5 cm s^{-1}), H_2O_2 (1.1 cm s^{-1}), organic peroxides (0.55 cm s^{-1}), methyl and ethyl nitrate (1.1 cm s^{-1}) and HCHO (0.33 cm s^{-1} and assumed the same for all other aldehydes). Dry deposition terms were calculated as V_i/h where V_i is the species-dependent dry deposition velocity and h is the (time-dependent) boundary layer

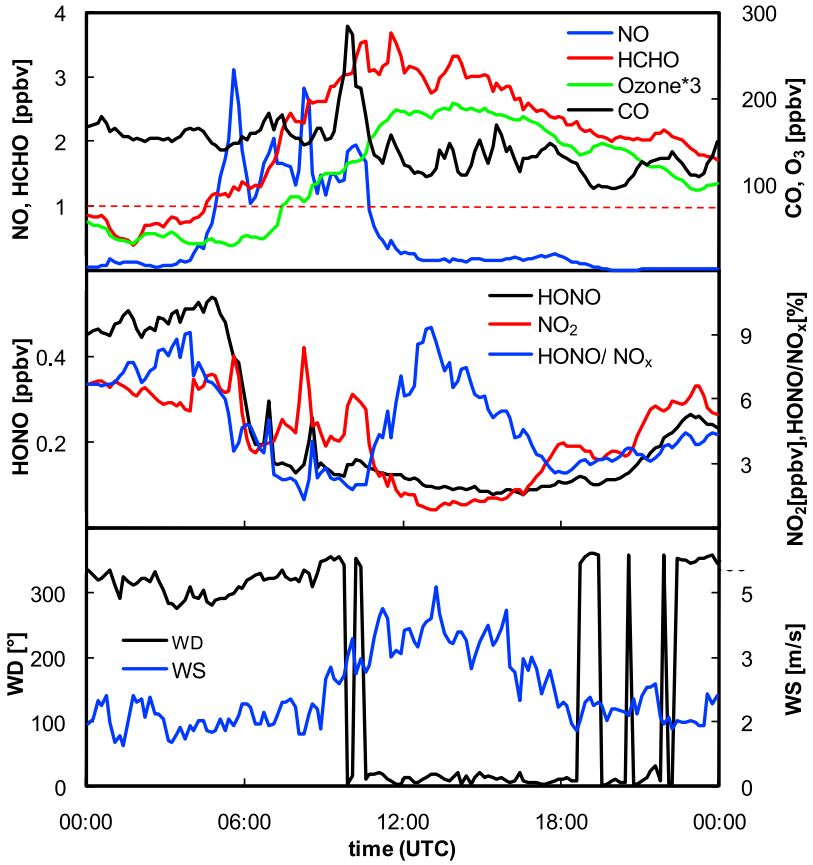

Figure 1. Ten minute average diurnal profiles of the measured parameters on 10 July during HOxComp. The red dashed line in Figure 1 (top) marks 1 ppbv NO. WD, wind direction; WS, wind speed.

mixing height. In the model, the boundary layer collapses to 300 m during the night at 20:00 UTC and starts to build up during the morning at 06:00 UTC, reaching a height of 1.3 km at 14:00 UTC. This boundary layer depth is maintained until early evening, when the nocturnal boundary layer of 300 m is reestablished. A series of rate of production analyses (ROPA) was carried out in order to identify the most important photochemical processes driving the formation and loss of OH and HO_2. The MCM photochemical model was run for a period of 5 days, constrained with the same measured campaign parameters each day, to generate realistic concentrations for the unmeasured intermediate species. By the fifth day, free radicals in the model have reached photostationary state. Output from day 5 is used for data evaluation. This model version is henceforth denoted as the base model. Owing to the very large number of reactions and parameters involved in MCMv3.2, it is difficult to determine the model errors. Here, we adopt the 1σ model errors for OH (17%) and HO_2 (16%) estimated by *Kanaya et al.* [2011] for the conditions encountered at noontime of 10 July during HOxComp. The model errors consider the propagation of uncertainties of the rate coefficients in a revised RACM based box model and also the errors of measured trace gases and photolysis frequencies used as model input. These uncertainties are also in good agreement with 2σ error for OH (42%) and HO_2 (25%), estimated previously using MCM under semi polluted conditions [*Carslaw et al.*, 1999]. Throughout this paper, production and destruction of a species X are referred to as P_x and L_x, respectively. P_x and L_x are defined such as $P_x(Y \rightarrow X)$ when X is produced from Y or by describing the reaction leading to production or loss of X such as $P_x(Y + Z)$.

3. Results and Discussion

3.1. Field Measurement Results

[13] As shown in Figure 1, two different air masses can be distinguished at the measurement site owing to different wind directions (WD), from the northwest (∼315°) carrying anthropogenic emissions from the nearby city of Jülich (see section 2.1) during the early morning until around 10:00 UTC, then turning more northerly (∼10°) with much higher wind speed reaching 5 m s^{-1} (see Figure 1) during the rest of the day. Caused by this and by additional diurnal variability of the boundary layer height and the ozone concentration, NO levels ranged from 1 to 3 ppbv during the early morning until around 10:00 UTC and then decreased to less than 1 ppbv during the rest of the day. Therefore, two different chemical regimes have been identified; hereafter referred to as high-NO_x (06:00–10:00 UTC) and low-NO_x (11:00–18:00 UTC) periods with average NO mixing ratios of 1.6 and 0.21 ppbv, respectively (see Figure 1). CO and NO_2 showed similar diurnal profiles with average mixing ratios of CO (171, 132 ppbv), NO_2, (4.65, 1.71 ppbv) during the high- and low-NO_x periods, respectively. In contrast, HCHO reached a broad maximum of 3.7 ppbv at 11:35 UTC,

Table 1. List of Measured Hydrocarbons During HOxComp on 10 July 2005

Compound	Average Mixing Ratio (ppbv)		
	06:00–10:00 UTC	11:00–18:00 UTC	06:00–18:00 UTC
Ethane	1.55	0.85	1.17
Propane	0.99	0.49	0.70
i-butane (2-methylpropane)	0.20	0.12	0.16
i-pentane (2-methylbutane)	0.37	0.23	0.29
n-pentane	0.20	0.13	0.16
n-hexane	0.08	0.05	0.06
n-heptane	0.04	0.02	0.03
n-octane	0.02	0.04	0.03
Ethene	0.53	0.18	0.32
Propene	0.31	0.11	0.18
i-butene (2-methylpropene)	0.07	0.05	0.06
trans-2-butene	0.04	0.02	0.03
cis-2-pentene	0.01	0.02	0.02
Isoprene	0.37	0.98	0.74
Ethine (acetylene)	0.18	0.10	0.13
Ethylbenzene	0.04	0.02	0.03
m- and p-xylene[a]	0.06	0.02	0.04
o-xylene	0.02	0.01	0.01
Toluene	0.29	0.11	0.20
Benzene	0.24	0.21	0.22
Butanal	$<D_L$	0.06	0.04
Butanone	0.28	0.13	0.19
Methacroleine	0.02	$<D_L$	0.01
Methylvinylketone	$<D_L$	0.11	0.07
Propanal	0.03	0.03	0.03
Acetone	2.17	3.77	3.16
Acetaldehyde	0.86	1.13	1.02

[a]Not constrained to the MCM.

1 h before the ozone maximum mixing ratio of 62 ppbv, due to contributions from secondary photochemical sources (Figure 1).

[14] The HONO/NO_x ratio showed two maxima (see Figure 1). While the typical nighttime maximum (around 04:00 UTC) can be explained by heterogeneous nighttime sources and the lack of photolysis of HONO, the second maximum during daytime (at around 14:00 UTC) points to a strong daytime source of HONO for which photochemical sources have been proposed [*Kleffmann et al.*, 2005; *Kleffmann*, 2007]. Similar diurnal profiles of the HONO/NO_x ratio were also observed under rural [e.g., *Acker et al.*, 2006], remote [e.g., *Kleffmann and Wiesen*, 2008], and urban conditions [e.g., *Elshorbany et al.*, 2009a, 2010a].

[15] A list of the average mixing ratios of the measured hydrocarbons is shown in Table 1. Measured compounds less than the detection limits ($<D_L$) were constrained to the model as zero values while those identified as mixture of two compounds or more were not constrained. The averaged diurnal profiles of VOCs (in parts per billion, ppbC) and NO_x (ppbv), in addition to the contribution of different species and VOC categories to the primary OH reactivity (see section 3.8) are shown in Figure 2. The relative contribution of the different VOCs during the high- and low-NO_x periods are alkanes (35, 20%), alkenes (8, 3), isoprene (6, 16%), acetylenes (1, 1%), aromatics (15, 8%) and OVOCs (35, 52%) to the total measured VOCs of about 30 and 31 ppbC, respectively. Unlike NO_x, the total amount of VOC is almost constant during the day. Thus, the VOC/NO_x ratio is about 5 during the high-NO_x period, but reaches a value of about 30 at 13:00 UTC (i.e., VOC-sensitive conditions at VOC/NO_x < 10 and NO_x sensitive conditions at VOC/NO_x > 20; see also section 3.3 [*National Research Council*, 1991]). In addition, since not all hydrocarbons could be measured by the GC analysis techniques used, similar to other field measurement studies [*Elshorbany et al.*, 2009a; *Dusanter et al.*, 2009, and references therein], a higher VOC/NO_x ratio is expected. The relative contribution of the different VOC categories to the primary OH reactivity (see Figure 2) varies during the daytime, depending on the NO_x levels. As expected, NO_x and anthropogenic emissions of alkanes, alkenes and aromatics had the highest contribution during the high-NO_x period (06:00–10:00 UTC) while isoprene, OVOCs and HCHO reached their highest contribution during the low-NO_x period (11:00–18:00 UTC). The OVOC category herein does not include HCHO, which is treated separately due to its particular importance.

[16] The measured diurnal profiles of both OH and HO_2 exhibit similar variations, with maximum values at noontime and concentrations near zero at night (Figures 3a and 3b). The red lines show the mean diurnal profiles measured by all instruments, while the gray area represents the range of measurements by the different instruments, which might be interpreted roughly as a measure of the experimental uncertainty (see section 2.2). The black lines represent the base model results, which show very good agreement (within ± 30%) with the experimental observations both for OH and HO_2. As pointed out in section 2.2, the measured HO_2 data contain uncorrected contributions by RO_2. The model calculated RO_2 concentrations from the base model

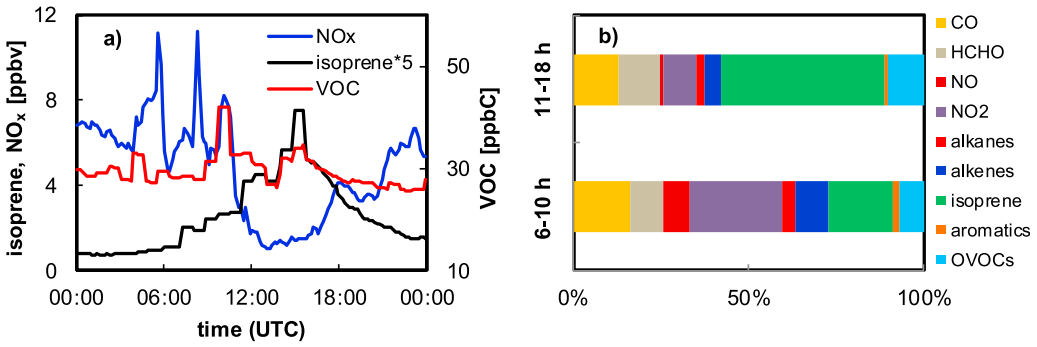

Figure 2. (a) Diurnal variation of measured isoprene, VOCs, and NO_x mixing ratios and (b) relative contributions of the different VOC categories and other species to the primary OH reactivity.

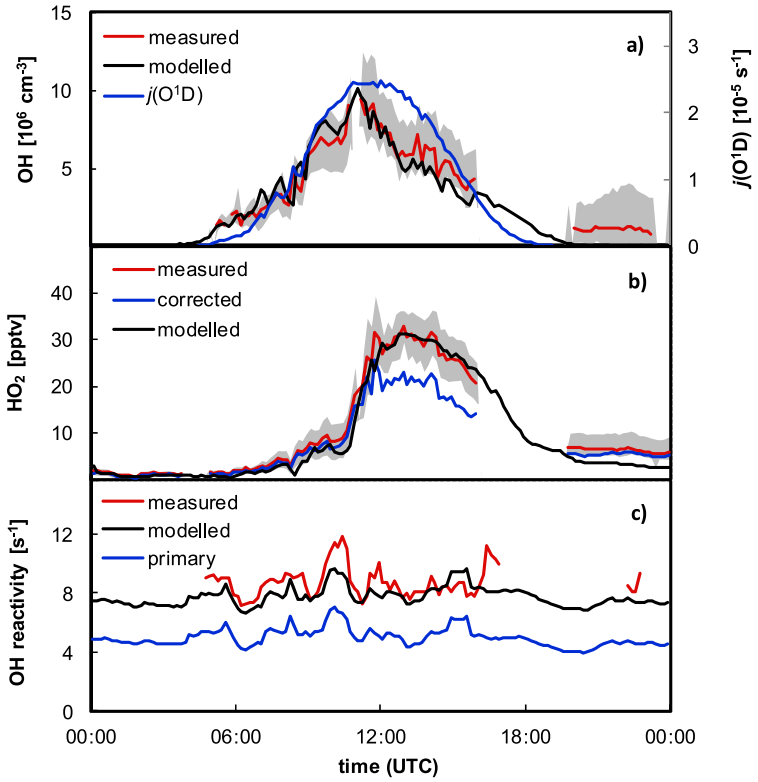

Figure 3. Ten minute average measured and modeled OH, HO_2, and OH reactivity as well as the corrected measured HO_2 levels due to interferences by RO_2 cross reactions on 10 July. Gray areas determine the minimum and maximum HO_x levels measured by different instruments.

run have been used to estimate the magnitude of this interference. Based on the cross sensitivities for the different RO_2 species determined for FZJ-LIF [*Fuchs et al.*, 2011], the possible bias is calculated to be +22% and +47% during the high- and low-NO_x periods, respectively. If we assume that the two other LIF instruments had similar interferences (i.e., cross sensitivities from RO_2 species determined for FZJ-LIF), then the measured HO_2 by FRCGC-LIF and MPI-LIF would have to be reduced by (26, 36)% and (10, 25)% during the high- and low-NO_x period, respectively. Accordingly, the mean corrected HO_2 data in Figure 3b are smaller than the uncorrected values by 14% at high-NO_x conditions and 26% at low-NO_x conditions. After the correction, the modeled HO_2 is still in good agreement with the observations in the morning (within the gray area) but overpredicts the corrected measured HO_2 by a factor of 1.3 to 1.8 during the low-NO_x period.

[17] Figure 3c shows the measured total OH reactivity (red line) which has a daytime average value of 8.8 ($\pm$0.8) s^{-1} reaching its maximum of 11.8 s^{-1} at about 10:00 UTC and minimum of 7.2 s^{-1} at about 06:00 UTC. About 60% of the measured reactivity can be explained by measured trace gases (blue line) during the daytime. A detailed discussion of the model-measurement comparisons for OH, HO_2 and OH reactivity is given in sections 3.5, 3.6 and 3.8.

3.2. Oxidation Capacity

[18] The oxidation capacity (OC) defined earlier is calculated from the total loss rates of the VOCs and CO due to reactions with OH, O_3 and NO_3 using the MCM model. The average oxidation capacity of OH, O_3 and NO_3 radicals throughout the entire day is 1.7×10^7, 8.6×10^6 and 1.8×10^6 molecule cm^{-3} s^{-1} representing about 63, 31, and 6% of the total oxidation capacity, respectively. During daytime (06:00–18:00 UTC), OH is also the dominant oxidant with an average oxidation rate of 3.3×10^7 molecules cm^{-3} s^{-1} followed by O_3 and NO_3 of 7.6×10^6 and 1.2×10^6 molecules cm^{-3} s^{-1} representing 79, 18 and 3% of the total OC, respectively. In contrast, during the night and early morning O_3 was the dominant oxidant. Owing to the dominant contribution of the OH radical to the OC during daytime, the current study focuses only on the HO_x chemistry analysis during HOxComp.

3.3. Modeled HO_x Budget

[19] The total production and destruction rates of OH and HO_2 calculated by the MCM model are shown in Figure 4a, with ratios of the radical production/destruction shown in Figure 4b. As expected, owing to the very short lifetime of HO_x radicals, the ratios of the total production to destruction of OH and HO_2 are around unity throughout the day, but highly fluctuating in the early morning due to the large variation of NO_x (see Figure 4b). In addition, for the hydroxyl radical the ratio reaches a maximum of about 1.6 during the early morning at 04:30 UTC, which may be due to the photolysis of nighttime accumulated HONO. During the high-NO_x period (06:00–10:00 UTC), when NO levels are > 1 ppbv (see red dotted line in Figure 4a), total production and destruction rates of OH and HO_2 were almost similar. However, when NO levels fall below 1 ppbv, OH

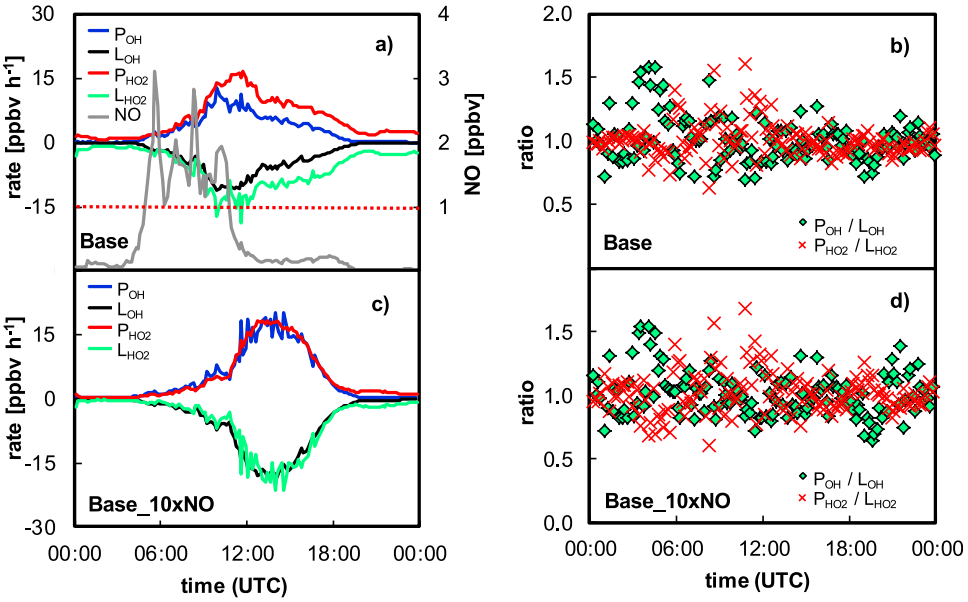

Figure 4. (a and c) Total production and destruction rates of OH and HO_2 and (b and d) ratio of production to destruction rates of OH and HO_2, using the base model (Figures 4a and 4b) in comparison to that of the Base_10xNO scenario (Figures 4c and 4d). The red dashed line in Figure 4a marks the 1 ppbv NO limit.

total production and destruction rates become much lower than those of HO_2. This is due to the lower recycling efficiency of HO_2 radicals (i.e., HO_2+NO→OH) during the low-NO_x period (see section 3.4). In order to further support the above argument, an additional sensitivity scenario was performed (Base_10×NO), in which the constrained NO concentrations were increased by a factor of 10. The reason for this is to increase the minimum measured NO concentrations of 0.1 ppbv during the daytime (06:00–10:00 UTC) to reach 1 ppbv, at which an efficient radical recycling (i.e., of HO_2 to OH) occurs (see above). As a result of increasing NO (Base_10×NO scenario) OH and HO_2 production and destruction rates become similar during the entire daytime owing to the increased recycling efficiency (Figure 4). Thus, the lower production and destruction rates of OH compared to those of HO_2 (see Figure 4) are consequences of the NO_x-limited conditions, which also lead to the unsymmetrical profiles observed for both, the measured and modeled OH (see section 3.2).

[20] The main RO_2 production term is due to hydrocarbon oxidation with OH (hereafter referred as $L_{OH}(OH \rightarrow RO_2)$) with an average rate of 2.6 and 3.8 ppbv h^{-1} during the high- and low-NO_x periods, which corresponds to about 50 and 70% of the total OH loss rate, respectively (see Figure 5). The main loss of RO_2 is due to its reaction with NO ($L_{RO2}(RO_2+NO)$) with average loss rates of 2.6 and 3.3 ppbv

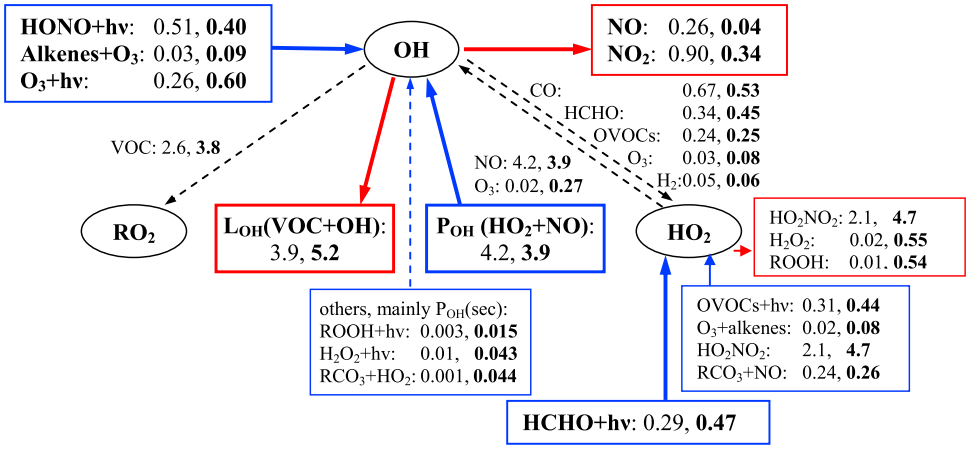

Figure 5. Average fluxes (06:00–18:00 UTC) of the key radical sources and sinks during HOxComp on 10 July calculated by the MCMv3.2 for the high-NO_x period in comparison to that of low-NO_x period (bold letters). The HONO photolysis (HONO+hv) represents the gross HONO photolysis (i.e., not the net HONO photolysis defined in the text as P_{OH}(HONO)). Units are in ppbv h^{-1}.

h^{-1} for high- and low-NO_x conditions, respectively, which accounts for most of the HO_2 production. Other important HO_2 sources (hereafter referred to as $L_{OH}(OH \rightarrow HO_2)$) are the reactions of OH with OVOCs, CO, O_3 and H_2 with summed average rates of 1.34 and 1.37 ppbv h^{-1} during the high- and low-NO_x periods, respectively (see Figure 5). The average production rates of HO_2 due to photolysis of HCHO ($P_{HO2}(HCHO+h)$) are 0.29 and 0.47 ppbv h^{-1} during the high- and low-NO_x periods, respectively (Figure 5). One major destruction route of HO_2 is through its reaction with NO ($L_{HO2}(HO_2+NO)$) with averages of 4.2 and 3.9 ppbv h^{-1}, which account for only 65 and 39% of the total HO_2 destruction rate (L_{HO2} (total)) during the high- and low-NO_x periods, respectively. This contribution is much lower than that of about 80% reported under urban high-NO_x conditions [*Elshorbany et al.*, 2009a]. Owing to the higher RO_2 and HO_2 concentrations during the low-NO_x period (see section 3.2), the relative contribution of the HO_2 self-reaction ($L_{HO2}(HO_2+HO_2)$ leading to H_2O_2 formation) and its cross reactions with RO_2 ($L_{HO2}(HO_2+RO_2)$ leading to ROOH formation) to the L_{HO2}(total) are about 20 and 40 times higher than during the high-NO_x period, respectively (see Figure 5). This demonstrates the importance of these reactions under low-NO_x conditions and therefore, they should be considered when calculating the radical loss budgets under these conditions. The HO_2 loss due to its reaction with O_3 accounts for only 0.3% of the L_{HO2}(total) during the high-NO_x period but about 3% during the low-NO_x period. Another important HO_2 destruction path is its reaction with NO_2 to form HO_2NO_2 with an average loss rates of 2.1 and 4.7 ppbv h^{-1} accounting for 32 and 47% of L_{HO2} (total) during the high- and low-NO_x periods, respectively (Figure 5). However, this loss path is essentially a reversible reaction that leads to HO_2 formation with similar rates.

[21] The main OH loss route is through its reaction with hydrocarbons, followed by reactions with NO and NO_2. The rates of OH destruction due to CO and hydrocarbons oxidation can be calculated using the following relationships:

$$L_{OH}(OH + VOC) \approx L_{OH}(\text{total}) - k_{NO_2+OH}[NO_2][OH] - k_{OH+NO}[NO][OH], \quad (2)$$

or alternatively [*Elshorbany et al.*, 2010a],

$$L_{OH}(OH + VOC) \approx L_{OH}(OH \rightarrow HO_2) + L_{OH}(OH \rightarrow RO_2). \quad (3)$$

The average loss rates of OH radicals by reaction with VOCs were similar for both equations and are 3.9 and 5.2 ppbv h^{-1}, representing 77 and 93% of the L_{OH}(total) during the high- and low-NO_x periods (see Figure 5), respectively. The rest of the OH loss is caused by its reaction with NO_x, accounting for 23 and 7% of L_{OH} (total) during the high- and low-NO_x periods (see Figure 5), respectively.

[22] OH production is dominated by the recycling reaction of HO_2 with NO, $P_{OH}(HO_2 \rightarrow OH)$:

$$P_{OH}(HO_2 \rightarrow OH) = k_{HO_2+NO}[HO_2][NO]. \quad (4)$$

The $P_{OH}(HO_2 \rightarrow OH)$ route accounts for 83 and 73% to P_{OH}(total), while production of OH due to HO_2 reaction with O_3 account for 0.4 and 5% during the high- and low-NO_x periods, respectively (see Figure 5), The next most important secondary OH sources are the reaction of RCO_3+HO_2, the photolysis H_2O_2 and the photolysis of ROOH and RCO_3H species (hereafter collectively called P_{OH}(ROOH+hv)) that result from RO_2 cross reactions with HO_2. The total contribution of these secondary sources (hereafter referred to as P_{OH}(sec)) accounts for only 0.2% of the P_{OH} (total) during the high-NO_x period, but about 2% during the low-NO_x period.

3.4. Radical Propagation

[23] In order to investigate the radical propagation balance between OH secondary radical loss ($L_{OH}(OH+VOC)$) and production ($P_{OH}(HO_2+NO)$), a balance ratio (BR) introduced by *Elshorbany et al.* [2010a] was calculated by the model. The BR ratio is defined as

$$BR = \frac{P_{OH}(HO_2 \rightarrow OH)}{L_{OH}(OH \rightarrow HO_2) + L_{OH}(OH \rightarrow RO_2).} \quad (5)$$

According to this balance ratio, a BR value of 1 indicates that secondary production and destruction of OH are balanced. A BR < 1 indicates that secondary radical production is smaller than destruction. The latter case may prevail under very low NO_x conditions, which may lead to a low radical recycling efficiency and consequently, low secondary OH production. The secondary production of radicals is higher than their secondary destruction if BR > 1.

[24] During HOxComp, a modeled BR ratio of 1.07 was obtained during the high-NO_x period (see Figure 5) indicating almost a balance between the secondary radical loss and production owing to the high recycling efficiency [*Elshorbany et al.*, 2010a]. However, during the low-NO_x period (11:00–18:00 UTC), a BR ratio of 0.75 was obtained, indicating net secondary radical loss due to a low recycling efficiency. In addition, under low-NO_x conditions, significant fraction (about 9%) of the OH radical recycling processes occur without NO through P_{OH}(sec) and $P_{OH}(HO_2+O_3)$. These recycling processes partially compensate the deficit in the OH budget as a result of the low-NO_x conditions. Including the other OH secondary sources (P_{OH}(sec) and $P_{OH}(HO_2+O_3)$) in the secondary production term in (5), lead to only a very small increase of 0.7% in the BR ratio to 1.08 during the high-NO_x period, whereas it increased the BR during the low-NO_x period by 11% to 0.82. These results confirm our previous conclusion of high recycling efficiency during the high-NO_x period and lower recycling efficiency during the low-NO_x period. This lower recycling efficiency is mainly due to the increased HO_2 loss due to the formation of H_2O_2 and ROOH (see Figure 5) as a result of the low-NO_x conditions. The total OH production to destruction ratio of unity (see section 3.3) is maintained by the higher OH initiation rate and the lower loss rate by reactions with NO_x during the low-NO_x period (see section 3.3). Thus, in contrast to the calculated turnover rates, based on measured HO_2, OH and OH reactivity (see section 3.3), the primary and secondary sources fill the deficit in the radical budgets during afternoon, thus maintaining the balance between total radical production and destruction (see section 3.3).

[25] The HO_2/OH ratio is also a measure of the recycling efficiency; a high HO_2/OH ratio is typical for clean air with low-NO_x conditions [e.g., *Mihelcic et al.*, 2003; *Ren et al.*,

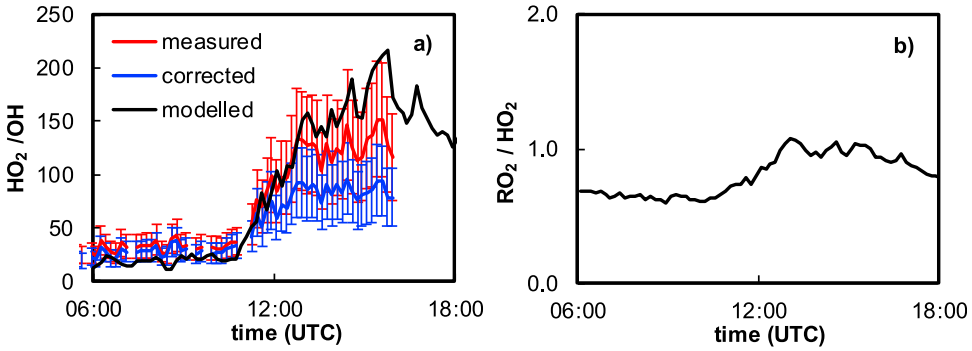

Figure 6. Diurnal profiles of modeled, measured, and corrected (for RO_2 interference) (a) HO_2/OH with 2σ error bars, calculated from the propagation error of the relative uncertainties of OH and HO_2 multiplied by the corresponding HO_2/OH ratio and (b) modeled RO_2/HO_2 during the daytime (06:00–18:00 UTC).

2005; *Hofzumahaus et al.*, 2009], while a low HO_2/OH ratio is typical for polluted air with high-NO_x conditions and implies a high recycling efficiency toward OH [e.g., *Elshorbany et al.*, 2009, and references therein]. The shape of the measured diurnal profile of the HO_2/OH ratio is well reproduced by the MCM model (see Figure 6) and values are within the measurements uncertainties (see section 3.1). However, if corrected HO_2 is used to calculate the HO_2/OH ratio, the agreement slightly improves during the high-NO_x period, but become significantly worse at low NO_x. This result shows that the cycling between OH and HO_2 is better described by the model at high NO_x than at low NO_x. The low modeled HO_2/OH ratio of 19 indicates high recycling efficiency during the high-NO_x period (06:00–10:00 UTC), but increases strongly during the low-NO_x period (11:00–18:00 UTC) with an average value of 125 (see Figure 6) indicating low recycling efficiency. This high HO_2/OH ratio is also in excellent agreement with that measured at Pearl River Delta, China [*Hofzumahaus et al.*, 2009], rural area of central Pennsylvania [*Ren et al.*, 2005], and BERLIOZ [*Mihelcic et al.*, 2003]. Modeled RO_2/HO_2 ratio ranges from 0.6 during the high-NO_x period to 1.0 during the low-NO_x period (Figure 6). The higher ratio during the low-NO_x period is also a result of the lower recycling efficiency during this period. In addition, the maximum total peroxy radical (RO_2+HO_2) concentrations of 65 pptv during the low-NO_x period (see Figure 7) is very high in comparison to other similar studies [*Mihelcic et al.*, 2003; *Hofzumahaus et al.*, 2009] and can be explained by the lower NO concentrations during HOxComp. The maxima in the diurnal profiles of RO_2 and HO_2 also coincide with the NO daytime minima as shown in Figure 7. This is also in agreement with the expected anticorrelation between the HO_2/OH ratio and NO as shown in Figure 7, which is in agreement with other studies [e.g., *Mihelcic et al.*, 2003]. The second peak in the RO_2 diurnal profile at around 20:00 UTC is due to the very low recycling efficiency (i.e., RO_2+NO→HO_2 and HO_2+NO→OH) owing to the extremely small NO values of about 0.01 ppbv at this time.

[26] To further investigate the recycling process, an additional MCM model scenario has been run, in which the concentrations of all constrained VOCs (except HCHO) have been increased by a factor of 2, referred to as Base_2×VOC. As shown in Figure 8, OH simulated by this scenario matched that simulated by the base model scenario during the high-NO_x period (within ± 2%), while it was lower by about 30% during the low-NO_x period compared to the base model scenario. The excellent agreement between the OH simulations by the base and base_2 × VOC scenarios during the high-NO_x condition is due to the high recycling efficiency during this time. This result shows that secondary OVOCs are not net sources of OH radicals, in excellent agreement with previous studies under polluted urban conditions [*Elshorbany et al.*, 2009a, 2010a]. The reduction in the OH levels as a result of increasing the VOC levels during the low-NO_x period is due to the NO-sensitive conditions, under which VOCs act as a net sink of OH

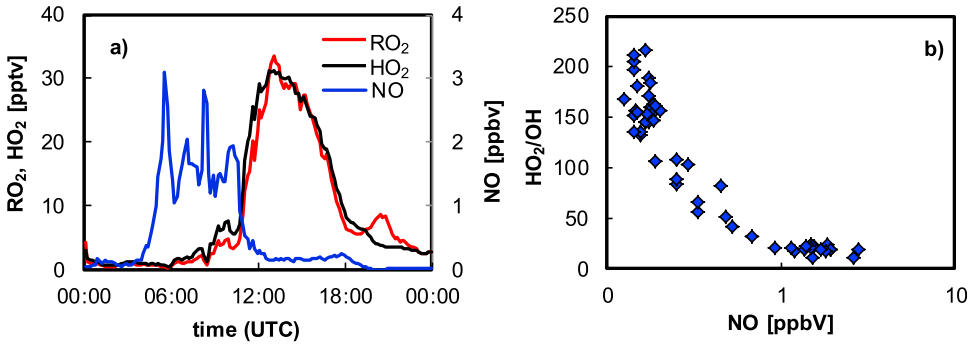

Figure 7. (a) Diurnal profiles of modeled HO_2 and RO_2 and (b) correlation between modeled HO_2/OH and NO.

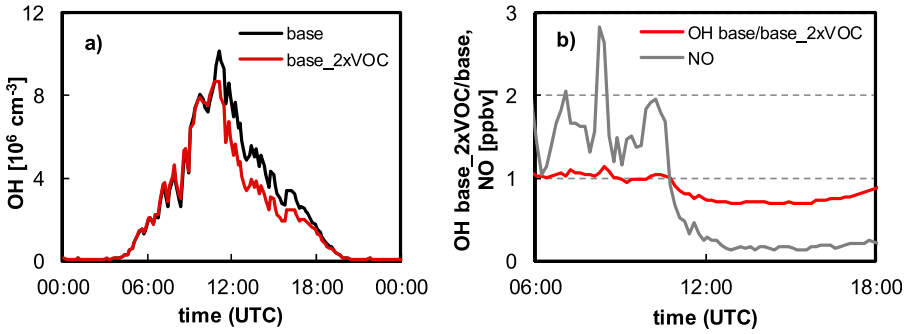

Figure 8. (a) Simulated diurnal profiles of OH of the base_2xVOC in comparison to the base model scenario and (b) ratio of the two simulated profiles with measured NO.

radicals due to the low recycling efficiency, in agreement with the conclusion given above.

[27] Very recently, *Mollner et al.* [2010] reported a more precise value for the rate constant k_{NO2+OH} of 9.2 (±0.4) × 10^{-12} cm^3 $molecule^{-1}$ s^{-1} at 25 °C and 1 atm of air, which is about 77% of the IUPAC values applied in the MCMv3.2 of $11.9^{+\ 6.0}_{-\ 3.0}$ × 10^{-12} cm^3 $molecule^{-1}$ s^{-1}. In order to test the impact of the new value of the k_{NO2+OH} on the simulated HO_x levels, an additional scenario was performed. As expected, only OH, HO_2 and RO_2 levels during the high-NO_x period were affected and increased by about 11%, while those during the low-NO_x period were increased by only about 3%. This is due to the high-NO_x conditions, for which NO_2 reaction with OH is the dominant sink of radicals (see section 3.3). Similarly, *Mollner et al.* [2010] reported a 10% increase in the O_3 levels as a result of using the new values of the k_{NO2+OH} rate constant, considering that O_3 instantaneous production rate is a function of HO_2 an RO_2 concentrations [e.g., *Elshorbany et al.*, 2009b].

3.5. Measured Versus Modeled Radical Levels

[28] The measured OH diurnal profile reached a maximum of 9.4 × 10^6 molecules cm^{-3} around noon at 11:15 UTC, about half an hour before the maximum $j(O^1D)$, shortly after the high-NO_x period, and then decreased sharply during the low-NO_x period owing to the lower recycling efficiency (see section 3.4). Owing to this different photochemical sensitivity during the daytime (i.e., high NO_x, 06:00–10:00 UTC and low NO_x, 11:00–18:00 UTC), measured and modeled OH diurnal profiles are asymmetric around the solar noon maximum (see Figure 3). This is due to the low-NO_x conditions during the time period 11:00–18:00 UTC, for which OH photostationary state equilibrium is shifted toward net OH loss by VOC oxidation (see section 3.4). The measured and modeled HO_2 diurnal profiles are also asymmetric and reach their maximum at about 13:00 UTC, around 1 h after the maximum of $j(O^1D)$. This is due to the high-NO_x levels which suppress the HO_2 levels only during the high-NO_x period in the morning (see Figure 3). In contrast to previous studies where modeled OH diurnal profiles were asymmetric, while that measured was symmetric around solar noon [e.g., *Emmerson et al.*, 2007; *Hofzumahaus et al.*, 2009], the asymmetrically distinctive features of the OH and HO_2 diurnal profiles during the high- and low-NO_x conditions were well reproduced by the MCMv3.2 box model in this study.

[29] The correlation between measured and modeled OH and HO_2 as well as the correlations of the ratio of measured/modeled values versus NO are shown in Figure 9. High correlations between measured and modeled OH and HO_2 values during daytime (06:00–18:00 UTC) with slopes around unity were obtained (see Figure 9). However, when the estimated interference caused by RO_2 cross reactions is considered, the slope between the corrected and modeled HO_2 regression line becomes 30% smaller, indicating a model overprediction of HO_2. Similar results were also obtained using RACM-based box model [*Kanaya et al.*, 2011]. The correlation between measured/modeled ratio of OH and HO_2 and NO (see Figure 9) shows that OH was slightly overestimated during the high-NO_x period but shows an increasing underestimation during the low-NO_x period, reaching 65% at <0.2 ppbv NO (see Figures 3 and 9). In contrast, HO_2 was underestimated during both, high- and low-NO_x periods by 48 and 17%, respectively. After correction of the HO_2 data for the interference by RO_2, the agreement improves slightly at NO values above 1 ppb, but a model overestimation of about 40% becomes apparent at low NO values of 0.2 ppb. Although there seem to be NO-dependent trends in the measured/modeled ratios of OH and HO_2, these trends must be considered carefully owing to the combined model and experimental errors, which are of the order of the observed deviations.

3.6. Experimental OH Budget

[30] The total OH production and loss rates determined from measured parameters are compared in Figure 10. The total OH production rate was calculated from the recycling rate of HO_2 (k_{NO+HO2} × [NO] × [HO_2]) in addition to the primary sources (P_R = j(HONO)[HONO] + $P_{OH}(O_3)$ + P_{OH}(alkenes); see section 3.7). The total OH loss rate was determined from the measured reactivity and concentration of OH (k_{OH} × [OH]). For OH and HO_2, the mean values of FRCGC_LIF and FZJ_LIF were used, while the data by MPI_LIF, which show much higher values (see section 2.2), were treated separately. The ratios of production to destruction of OH (P_{OH}/L_{OH}) are also shown in Figure 10 for both cases.

[31] When the OH and HO_2 data by FRCGC/FZJ are used (Figure 10), the OH loss rate is found to be almost balanced with the OH production rate at high-NO_x condition in the morning (P_{OH}/L_{OH} = 0.93), indicating a closed OH budget. During the low-NO_x period, however, the production rate is

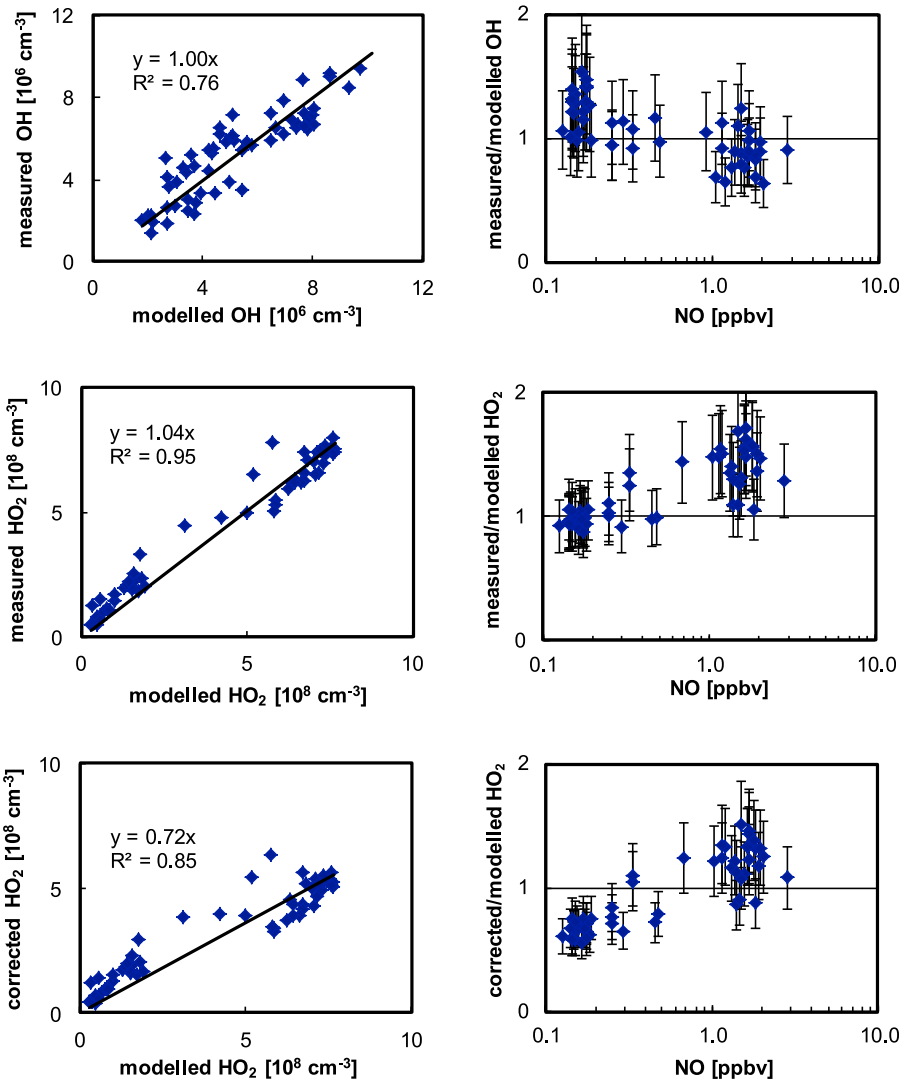

Figure 9. Correlation between measured and modeled (top) OH, (middle) HO_2, and (bottom) corrected HO_2 as well as the correlations of their ratios with NO (on a logarithmic scale) measured during HOxComp. Error bars represent 2σ relative error of the average measured OH and HO_2 levels.

smaller than the loss rate (P_{OH}/L_{OH} = 0.71), indicating the need for an additional OH source. When the OH and HO_2 data by MPI_LIF are considered (Figure 10), the OH production rate is found to be consistently larger than the OH sinks in the morning (P_{OH}/L_{OH} = 1.83). This result is hard to explain, given the expected high recycling efficiency during the high-NO_x period (see section 3.4), except by systematic errors of the calculated OH budget. At low NO_x, the production rate is smaller than the loss rate (P_{OH}/L_{OH} = 0.61), indicating a missing OH source, in qualitative agreement with the result from FRCGC/FZJ (Figure 10). The calculated gap during the low-NO_x period corresponds to 2.5 and 3.7 ppb h^{-1} on average of unaccounted OH sources for FRCGC/FZJ and MPI, respectively. The deficit in the OH budget becomes more apparent when the HO_2 data are corrected for the estimated interferences from RO_2. As shown in Figure 10, the P_{OH}/L_{OH} ratios calculated using corrected HO_2, decrease to 0.52 and 0.49 on average for FRCGC/FZJ and MPI, respectively, in average during the low-NO_x period. Consequently, the deficit in the OH budget increases to reach 3.6 and 4.9 ppb h^{-1} for FRCGC/FZJ and MPI, respectively, on average during the low-NO_x period. The experimental uncertainty of the missing OH source is about 45%, which represents the error propagation of the uncertainties of the parameters needed for calculation of the turnover rates (see section 2.2). It should be noted here that the result is particularly sensitive to the uncertainty of the HO_2 measurements (and the corrections), because the HO_2+NO reaction dominates the OH production rate (>70%; see section 3.3). The existence of a missing OH source during HOxComp agrees with findings from other field campaigns in isoprene-rich air at low NO_x, where efficient OH recycling without NO has been postulated as an additional OH source [*Lelieveld et al.*, 2008; *Hofzumahaus et al.*, 2009; *Lu et al.*, 2011; *Whalley et al.*, 2011].

3.7. OH Initiation Sources

[32] OH radical initiation describe processes that lead to the production of new OH radicals which include O_3 photolysis, $P_{OH}(O_3)$, HONO photolysis, P_{OH}(HONO),

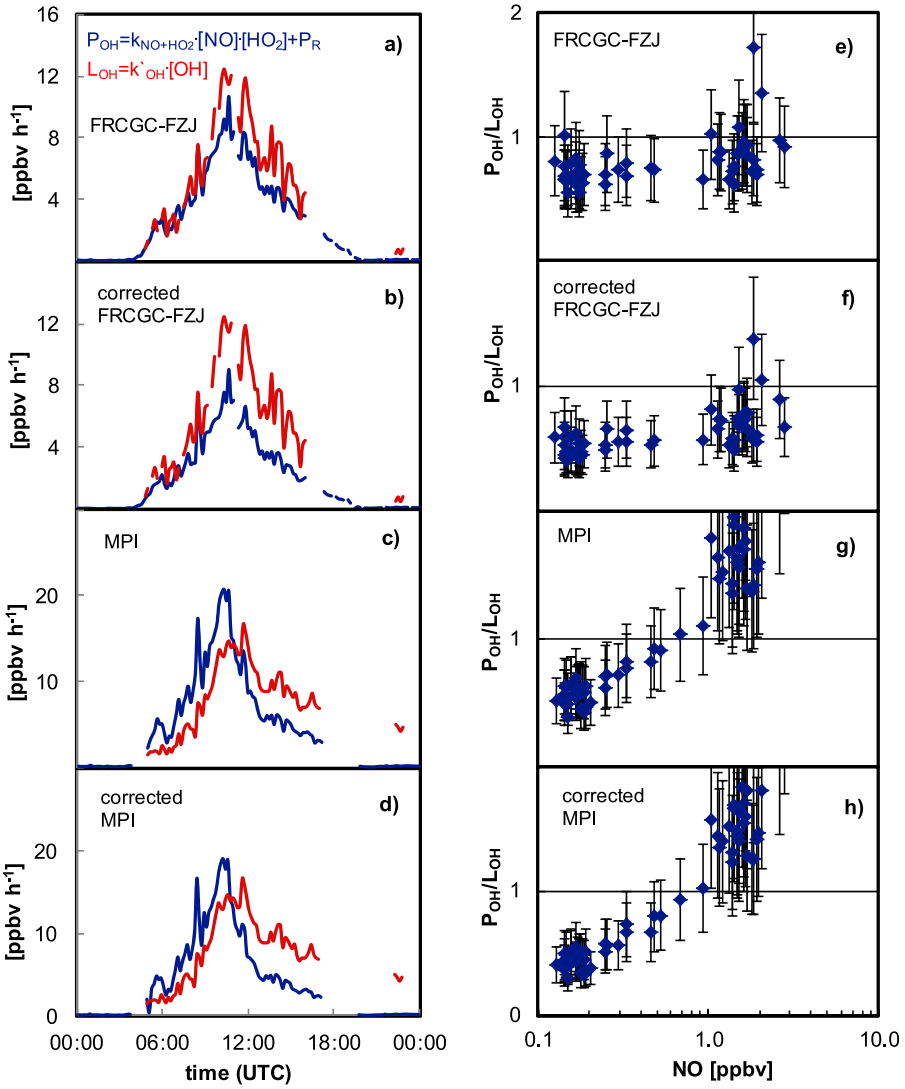

Figure 10. Calculated total OH loss (red, $k'_{OH}\cdot[OH]$) and production rates (blue, $k_{OH+HO2}\cdot[HO_2]\cdot[NO] + P_R$, with $P_R = j(HONO)\cdot[HONO] + P_{OH}(O_3) + P_{OH}(alkenes)$). Measured OH and HO_2 data from (a) FZJ_LIF and FRCGC_LIF (mean) and (c) MPI used in the calculations. (b) and (d) The corresponding HO_2 data corrected for the recently observed RO_2 interferences of the HO_2 instruments. (e–h) The ratio of production to destruction for each case with the 2σ error bars representing the propagation error of the experimental uncertainties of the parameters used for the calculation.

alkene ozonolysis, $P_{OH}(alkenes)$. For HONO photolysis, $P_{OH}(HONO)$, is given by

$$P_{OH}(HONO) = j(HONO)[HONO] - k_{OH+NO}[NO][OH], \quad (6)$$

for which only the net OH source rather than the gross HONO photolysis rate is considered. The photostationary state concentration of HONO, $[HONO]_{PSS}$, defined as

$$[HONO]_{PSS} = k_{OH+NO}[OH][NO]/(j(HONO) + k_{OH+HONO}[OH]), \quad (7)$$

accounts for about 44% of the measured HONO on average during the high-NO_x period, in comparison to only 9% during the low-NO_x period.

[33] The average absolute and relative diurnal contributions of the different net OH sources are shown in Figure 11. During the high- and low-NO_x periods, the photolytic sources, namely, photolysis of O_3 (48, 57)% and HONO (46, 34)%, have the highest contributions while alkene ozonolysis contribute only 6 and 9%, respectively. As shown in Figure 11, HONO photolysis has the highest contribution during the early morning but decreases gradually to reach its minimum of about 23% at 10:00 UTC. The relative contribution of HONO photolysis increases slightly after 10:00 UTC owing to the decreased $[HONO]_{PSS}$ levels as a result of decreased NO concentrations. The relative contribution of $P_{OH}(HONO)$ becomes stable until around 14:00 UTC, where its relative contribution increases again due to the lower contribution from O_3 photolysis. During daytime (06:00–18:00 UTC) photolysis of O_3 had the highest contribution of 56% followed by photolysis of HONO (36%) and alkene ozonolysis (8%).

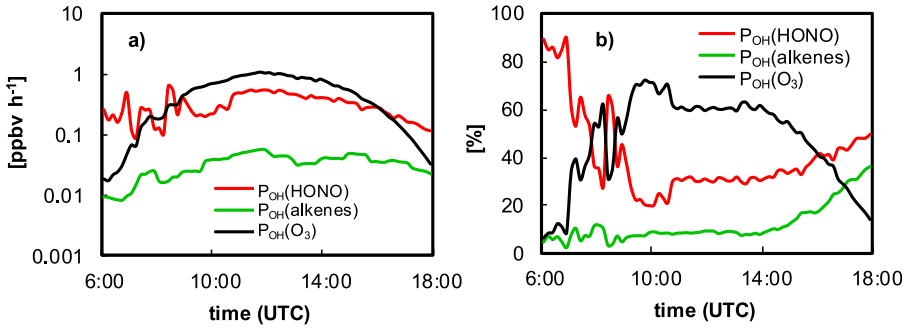

Figure 11. (a) Primary OH production rates from different sources (logarithmic scale) and (b) their relative contribution. $P_{OH}(HONO)$ represents the net HONO photolysis rate defined as $P_{OH}(HONO) = j(HONO)\cdot[HONO] - k_{OH+NO}\cdot[NO]\cdot[OH]$.

[34] Based on the correlation between the net OH formation by photolysis of HONO, $P_{OH}(HONO)$, and the photolysis frequencies, $j(NO_2)$ and $j(O^1D)$, and their different wavelength range *Elshorbany et al.* [2009a] postulated that the photolysis of nitric acid is a minor HONO source under urban conditions. Instead, photolytic sources active at longer wavelengths, like photosensitized conversion of NO_2 on humic acid surfaces [e.g., *Stemmler et al.*, 2006] or photolysis of nitroaromatic compounds [*Bejan et al.*, 2006], were proposed to be of higher importance. Similarly, analysis for the semirural conditions of this study (see Figure 12) confirms these results. The correlations in Figure 12 show that net HONO formation during the afternoon period is linearly dependent on $j(NO_2)$ and shows no significant intercept while the correlation is clearly curved for $j(O^1D)$. This can be explained by the much broader diurnal profile of $j(NO_2)$ compared to $j(O^1D)$. Thus, a short-wavelength range photochemical net HONO source [*Zhou et al.*, 2003, 2011] can most probably be excluded for the HOxComp campaign. It worth also noting that HONO formation was recently reported by *Su et al.* [2011] to be a function of temperature (also under dark conditions) rather than being light-dependent at all. Thus, further investigations of HONO daytime sources are still urgently needed.

3.8. OH Reactivity

[35] The diurnal profiles of measured and modeled OH reactivity are shown in Figure 3. The modeled OH reactivity, defined as the reciprocal of the OH radical lifetime, has been calculated from

$$\text{OH reactivity} = \frac{L_{OH}(\text{total})}{[OH]}. \quad (8)$$

The measured OH reactivity during daytime is well reproduced by the model within ± 14% (see Figure 3). The average modeled reactivities during the high- and low-NO_x periods of 7.7 s^{-1} and 8.2 s^{-1} are in good agreement (within the experimental uncertainties, see section 2.2) with those measured of 8.6 s^{-1} and 8.6 s^{-1} (see Figure 3). The calculated primary OH reactivity based solely on the measured species (9) of 5.3 s^{-1} and 5.2 s^{-1} is much lower than that measured by 38 and 40% during the high- and low-NO_x periods, respectively (see Figure 3):

$$\text{primary OH reactivity} = \Sigma\, k_{OH+Y_i}\cdot[Y_i], \quad (9)$$

where k_{OH+Yi} is the bimolecular rate constant for the reaction of Y_i with OH. A sensitivity test running the base model with and without isoprene as input shows that the enhancement of the modeled reactivity in Figure 3 relative to the primary OH reactivity is mainly caused by model-calculated isoprene degradation products. In another test, isoprene was constrained in the model, but all isoprene oxidation products (e.g., MACR, MVK, and HCHO) were unconstrained. In this case, the modeled concentrations of the isoprene products were found to be significantly larger by varying

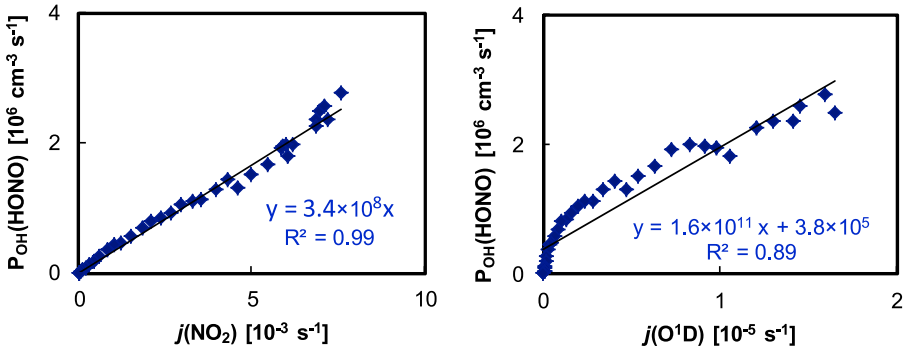

Figure 12. Correlation between $P_{OH}(HONO)$ and (a) $j(NO_2)$ and (b) $j(O^1D)$ during the afternoon (14:30–20:30 UTC). The linear regression shows that net HONO formation during the afternoon period is linearly dependent on $j(NO_2)$ and shows no significant intercept, while the correlation is clearly curved for $j(O^1D)$.

degrees than the corresponding measured values. One possible reason could be that most of the isoprene, which was freshly emitted by the forest around the measurement site, was less photochemically aged than implicitly assumed by the base model. As expected, owing to the increased levels of simulated OVOC, HO_2 and RO_2 and OH reactivity were also increased by different degrees. However, the increase in $P_{OH}(HO_2+NO)$ was almost compensated with the increase in the OH reactivity resulting in only slight changes in the OH levels. In addition, unmeasured, unconstrained isoprene secondary oxidation products, especially the organic peroxide of isoprene (ISOOH) that results from the reaction of the corresponding isoprene peroxy radicals (ISO_2) with HO_2, may react with OH at a rate constant that is comparable to that of isoprene and therefore contributes significantly to the OH reactivity and production [e.g., *Kubistin et al.*, 2010; *Pugh et al.*, 2010]. In very clean, pristine air, *Kubistin et al.* [2010] showed explicitly that measured ISOOH reaction with OH contributes 15% to both the total OH loss and production and thus has no net effect on the OH budget. These results are in agreement with our previous studies that showed that photochemically formed OVOCs are not a net OH source [*Elshorbany et al.*, 2009a, 2010b]. Thus, the uncertainty due to the local isoprene emission has little influence on the OH prediction, but causes a possible bias in modeled HO_2, RO_2 and OH reactivity. A RACM-based box model with updated isoprene chemistry was found to significantly underestimate the measured OH reactivity by 2.5 s^{-1}, on average during daytime on 10 July, for which several sensitivity analyses were performed to account for this missed OH reactivity [*Kanaya et al.*, 2011].

[36] Similar to the HOxComp campaign, other studies have also found that the OH reactivity calculated from only measured trace gases underestimates the measured [e.g., *Di Carlo et al.*, 2004; *Yoshino et al.*, 2006; *Ren et al.*, 2006; *Lou et al.*, 2010; *Lee et al.*, 2009; *Mogensen et al.*, 2011] or modeled [*Elshorbany et al.*, 2009a] total OH reactivity. At HOxComp, the OH reactivity split of NO_x, O_3, CO, HCHO and OVOCs was determined from their total loss rates due to reaction with OH (calculated by the base model, see Figure 5 and equation (8). The OH reactivity of NO_x accounts for 23 and 7% of the total reactivity during the high- and low-NO_x periods, respectively. Among the VOCs, isoprene and its oxidation products had the highest contribution to the total OH reactivity of 31 and 51% during the high- and low-NO_x periods followed by CO (13, 10)%, HCHO (7, 8)%, OVOCs (5, 4)%, O_3 (1, 2)% and other VOCs (20, 18)%, respectively. It should also be mentioned that biogenic hydrocarbons (including monoterpenes and sesquiterpenes) other than isoprene are emitted by the forest trees at Forschungszentrum Jülich. For example, *Dlugi et al.* [2010] reported measured values of about 200 ppt of monoterpenes for July 2003, which may add reactivity of the order of 0.5 s^{-1}. During HOxComp, monoterpenes were not measured in ambient air and are therefore not considered in the model here.

3.9. Conclusion

[37] In this study HO_x chemistry under NO_x-limited conditions was investigated through detailed analysis of the radical budgets using the master chemical mechanism, MCMv3.2. The model results have been compared and contrasted with measured radical levels performed simultaneously by different techniques during the international blind HOxComp intercomparison campaign.

[38] Both modeled OH and HO_2 diurnal profiles lay within the measurement range of all HO_x measurement techniques with correlation slopes between mean measured and modeled OH and HO_2 values of about unity during daytime (06:00–18:00 UTC). However, when the estimated interference caused by RO_2 cross reactions is considered, the slope between the corrected and modeled HO_2 regression line becomes 30% smaller, indicating a model overprediction of HO_2. The correlation between measured/modeled ratio of OH and HO_2 and NO shows that OH was slightly overestimated during the high-NO_x period but shows an increasing underestimation during the low-NO_x period, reaching 65% at <0.2 ppbv NO. In contrast, HO_2 was underestimated during both, high- and low-NO_x periods by 48 and 17%, respectively. After correction of the HO_2 data for their interference by RO_2, the agreement improves slightly at NO values above 1 ppbv, but a model overestimation of about 40% becomes apparent at low NO values of 0.2 ppbv. In addition, a missing OH source 2.5 and 3.7 ppb h^{-1} on average during the low-NO_x period for FRCGC/FZJ and MPI, respectively, was estimated from the calculated OH budget during the low-NO_x period. The deficit in the OH budget becomes more apparent when the HO_2 data are corrected for the estimated interferences from RO_2, reaching 3.6 and 4.9 ppb h^{-1} for FRCGC/FZJ and MPI, respectively, on average during the low-NO_x period. This missing OH source is in qualitative agreement with other previous studies but quantitatively much lower.

[39] The impact of the reported more precise values of k_{NO2+OH} was estimated and found to increase the measured HO_x levels only during the high-NO_x period by 11%.

[40] During the high- and low-NO_x periods, the photolytic radical initiation sources, namely, photolysis of O_3 (48, 57)%, and HONO (46, 34)% contributed most, while alkene ozonolysis contributed only 6 and 9%, respectively.

[41] The average modeled reactivities during the high- and low-NO_x periods of 7.7 and 8.2 s^{-1} are in good agreement with those measured. Among the VOCs, isoprene and its degradation products had the highest contribution to the total OH reactivity of 31 and 51% during the high- and low-NO_x periods followed by CO (13, 10)%, HCHO (7, 8)%, OVOCs (5, 4)%, O_3 (1, 2)% and other VOCs (20, 18)%, respectively.

[42] A BR ratio near unity was obtained during the high-NO_x period (06:00–10:00 UTC), indicating a balance between the secondary radical loss and production owing to the high recycling efficiency. However, during the low-NO_x period (11:00–18:00 UTC), a BR ratio of only 0.75 was obtained indicating net secondary radical loss due to a low recycling efficiency. In addition, under low-NO_x conditions, a significant fraction of the OH radical recycling processes occur without NO through $P_{OH}(sec)$ and $P_{OH}(HO_2+O_3)$. These recycling processes partially compensate the deficit in the OH budget as a result of the low-NO_x conditions. Thus, in contrast to the experimental OH budget calculated based on measured HO_2, OH and OH reactivity, the initiation sources and other modeled secondary sources fill the deficit in the radical budgets during afternoon, thus maintaining the balance between total radical production and destruction. The measured diurnal profile of the HO_2/OH ratio is well reproduced by the MCM model within the measurement

uncertainties. However, if corrected HO_2 is used to calculate the HO_2/OH ratio, the agreement slightly improves during the high-NO_x period, but becomes significantly worse at low NO_x. This result shows that the cycling between OH and HO_2 is better described by the model at high NO_x than at low NO_x. Similar field model comparison studies are still urgently needed to investigate HO_x recycling under NO_x-limited conditions.

[43] **Acknowledgments.** This work was supported by the EU FP-6 program EUROCHAMP (Integration of European Simulation Chambers for Investigating Atmospheric Processes, grant RII3-CT-2004-505968) and ACCENT (Priority 1.1.6.3. Global Change and Ecosystems, grant GOCECT-2004-505337). We thank F. J. Johnen for assistance with the experiments.

References

Acker, K., D. Möller, W. Wieprecht, F. X. Meixner, B. Bohn, S. Gilge, C. Plass-Dülmer, and H. Berresheim (2006), Strong daytime production of OH from HNO_2 at a rural mountain site, *Geophys. Res. Lett.*, *33*, L02809, doi:10.1029/2005GL024643.

Bejan, I., Y. Abd El Aal, I. Barnes, T. Benter, B. Bohn, P. Wiesen, and J. Kleffmann (2006), The photolysis of ortho-nitrophenols: A new gas phase source of HONO, *Phys. Chem. Chem. Phys.*, *8*, 2028–2035, doi:10.1039/b516590c.

Bloss, C., V. Wagner, A. Bonzanini, M. E. Jenkin, K. Wirtz, M. Martin-Reiejo, and M. J. Pilling (2005a), Evaluation of detailed aromatic mechanisms (MCMv3 and MCMv3.1) against environmental chamber data, *Atmos. Chem. Phys.*, *5*, 623–639, doi:10.5194/acp-5-623-2005.

Bloss, C., et al. (2005b), Development of a detailed chemical mechanism (MCMv3.1) for the atmospheric oxidation of aromatic hydrocarbons, *Atmos. Chem. Phys.*, *5*, 641–664, doi:10.5194/acp-5-641-2005.

Carslaw, N., D. J. Creasey, D. E. Heard, A. C. Lewis, J. B. McQuaid, M. J. Pilling, P. S. Monks, B. J. Bandy, and S. A. Penkett (1999), Modeling OH, HO_2 and RO_2 radicals in the marine boundary layer: 1. Model construction and comparison with field measurements, *J. Geophys. Res.*, *104*, 30,241–30,255, doi:10.1029/1999JD900783.

Curtis, A. R., and W. P. Sweetenham (1987), FACSIMILE Release H User's Manual, *AERE Rep. R11771*, HMSO, London.

Di Carlo, P., et al. (2004), Missing OH reactivity in a forest: Evidence for unknown reactive biogenic VOCs, *Science*, *304*, 722–725, doi:10.1126/science.1094392.

Dlugi, R., et al. (2010), Turbulent exchange and segregation of HO_x radicals and volatile organic compounds above a deciduous forest, *Atmos. Chem. Phys.*, *10*, 6215–6235, doi:10.5194/acp-10-6215-2010.

Dusanter, S., et al. (2009), Measurements of OH and HO_2 concentrations during the MCMA-2006 field campaign - Part 2: Model comparison and radical budget, *Atmos. Chem. Phys.*, *9*, 6655–6675, doi:10.5194/acp-9-6655-2009.

Elshorbany, Y. F., R. Kurtenbach, P. Wiesen, E. Lissi, M. Rubio, G. Villena, E. Gramsch, A. R. Rickard, M. J. Pilling, and J. Kleffmann (2009a), Oxidation capacity of the city air of Santiago, Chile, *Atmos. Chem. Phys.*, *9*, 2257–2273, doi:10.5194/acp-9-2257-2009.

Elshorbany, Y. F., J. Kleffmann, R. Kurtenbach, M. Rubio, E. Lissi, G. Villena, E. Gramsch, A. R. Rickard, M. J. Pilling, and P. Wiesen (2009b), Summertime photochemical ozone formation in Santiago, Chile, *Atmos. Environ.*, *43*, 6398–6407, doi:10.1016/j.atmosenv.2009.08.047.

Elshorbany, Y. F., J. Kleffmann, R. Kurtenbach, E. Lissi, M. Rubio, G. Villena, E. Gramsch, A. R. Rickard, M. J. Pilling, and P. Wiesen (2010a), Seasonal dependence of the oxidation capacity of the city of Santiago de Chile, *Atmos. Environ.*, *44*, 5383–5394, doi:10.1016/j.atmosenv.2009.08.036.

Elshorbany, Y. F., I. Barnes, K. H. Becker, J. Kleffmann, and P. Wiesen (2010b), Sources and cycling of tropospheric hydroxyl radicals—An overview, *Z. Phys. Chem.*, *224*, 967–987, doi:10.1524/zpch.2010.6136.

Emmerson, K. M., et al. (2007), Free radical modelling studies during the UK TORCH Campaign in summer 2003, *Atmos. Chem. Phys.*, *7*, 167–181, doi:10.5194/acp-7-167-2007.

Fuchs, H., et al. (2010), Technical note: Formal blind intercomparison of HO_2 measurements in the atmosphere simulation chamber SAPHIR during the HOxComp campaign, *Atmos. Chem. Phys.*, *10*, 12,233–12,250, doi:10.5194/acp-10-12233-2010.

Fuchs, H., B. Bohn, A. Hofzumahaus, F. Holland, K. D. Lu, S. Nehr, F. Rohrer, and A. Wahner (2011), Detection of HO_2 by laser-induced fluorescence: Calibration and interferences from RO_2 radicals, *Atmos. Meas. Tech.*, *4*, 1209–1225, doi:10.5194/amt-4-1209-2011.

Geiger, H., I. Barnes, I. Bejan, T. Benter, and M. Spittler (2003), The tropospheric degradation of isoprene: An updated module for the regional atmospheric chemistry mechanism, *Atmos. Environ.*, *37*, 1503–1519, doi:10.1016/S1352-2310(02)01047-6.

Geyer, A., B. Alicke, S. Konrad, T. Schmitz, J. Stutz, and U. Platt (2001), Chemistry and oxidation capacity of the nitrate radical in the continental boundary layer near Berlin, *J. Geophys. Res.*, *106*, 8013–8025, doi:10.1029/2000JD900681.

Hayman, G. D. (1997), Effects of Pollution Control on UV Exposure, *AEA Technol. Final Rep. AEA/RCEC/22522001/R/002 Issue 1*, AEA Technol., Didcot, U. K.

Hofzumahaus, A., et al. (2009), Amplified trace gas removal in the troposphere, *Science*, *324*(5935), 1702–1704, doi:10.1126/science.1164566.

Jenkin, M. E., S. M. Saunders, and M. J. Pilling (1997), The tropospheric degradation of volatile organic compounds: A protocol for mechanism development, *Atmos. Environ.*, *31*, 81–104, doi:10.1016/S1352-2310(96)00105-7.

Jenkin, M. E., S. M. Saunders, V. Wagner, and M. J. Pilling (2003), Protocol for the development of the Master Chemical Mechanism, MCM V3 (Part B): Tropospheric degradation of aromatic volatile organic compounds, *Atmos. Chem. Phys.*, *3*, 181–193, doi:10.5194/acp-3-181-2003.

Kanaya, Y., et al. (2011), Comparisons of observed and modeled OH and HO_2 concentrations during the ambient measurement period of the HOxComp field campaign, *Atmos. Chem. Phys. Discuss.*, *11*, 28,851–28,894, doi:10.5194/acpd-11-28851-2011.

Karl, M., H.-P. Dorn, F. Holland, R. Koppmann, D. Poppe, L. Rupp, A. Schaub, and A. Wahner (2006), Product study of the reaction of OH radicals with isoprene in the atmosphere simulation chamber SAPHIR, *J. Atmos. Chem.*, *55*, 167–187, doi:10.1007/s10874-006-9034-x.

Kleffmann, J. (2007), Daytime sources of nitrous acid (HONO) in the atmospheric boundary layer, *ChemPhysChem*, *8*, 1137–1144, doi:10.1002/cphc.200700016.

Kleffmann, J., and P. Wiesen (2008), Technical note: Quantification of interferences of wet chemical HONO LOPAP measurements under simulated polar conditions, *Atmos. Chem. Phys.*, *8*, 6813–6822, doi:10.5194/acp-8-6813-2008.

Kleffmann, J., T. Gavriloaiei, A. Hofzumahaus, F. Holland, R. Koppmann, L. Rupp, E. Schlosser, M. Siese, and A. Wahner (2005), Daytime formation of nitrous acid: A major source of OH radicals in a forest, *Geophys. Res. Lett.*, *32*, L05818, doi:10.1029/2005GL022524.

Kubistin, D., et al. (2010), Hydroxyl radicals in the tropical troposphere over the Suriname rainforest: Comparison of measurements with the box model MECCA, *Atmos. Chem. Phys.*, *10*, 9705–9728, doi:10.5194/acp-10-9705-2010.

Lee, G. D., et al. (2009), Measurement and calculation of OH reactivity at a United Kingdom coastal site, *J. Atmos. Chem.*, *64*, 53–76, doi:10.1007/s10874-010-9171-0.

Lelieveld, J., et al. (2008), Atmospheric oxidation capacity sustained by a tropical forest, *Nature*, *452*, 737–740, doi:10.1038/nature06870.

Levy, H. (1971), II Normal atmosphere: Large radical and formaldehyde concentrations predicted, *Science*, *173*, 141–143, doi:10.1126/science.173.3992.141.

Lockwood, A. L., P. B. Shepson, M. N. Fiddler, and M. Alaghmand (2010), Isoprene nitrates: Preparation, separation, identification, yields, and atmospheric chemistry, *Atmos. Chem. Phys.*, *10*, 6169–6178, doi:10.5194/acp-10-6169-2010.

Lou, S., et al. (2010), Atmospheric OH reactivities in the Pearl River Delta —China in summer 2006: Measurement and model results, *Atmos. Chem. Phys.*, *10*, 11,243–11,260, doi:10.5194/acp-10-11243-2010.

Lu, K. D., et al. (2011), Observation and modelling of OH and HO_2 concentrations in the Pearl River Delta 2006: A missing OH source in a VOC rich atmosphere, *Atmos. Chem. Phys. Discuss.*, *11*, 11,311–11,378, doi:10.5194/acpd-11-11311-2011.

Mihelcic, D., et al. (2003), Peroxy radicals during BERLIOZ at Pabstthum: Measurements, radical budgets and ozone production, *J. Geophys. Res.*, *108*(D4), 8254, doi:10.1029/2001JD001014.

Mogensen, D., et al. (2011), Modelling atmospheric OH-reactivity in a boreal forest ecosystem, *Atmos. Chem. Phys.*, *11*, 9709–9719, doi:10.5194/acp-11-9709-2011.

Mollner, A. K., et al. (2010), Rate of gas phase association of hydroxyl radical and nitrogen dioxide, *Science*, *330*, 646–649, doi:10.1126/science.1193030.

Mount, G. H., and E. G. Williams (1997), An overview of the tropospheric OH photochemistry experiment, Fritz Peak/Idaho Hill, Colorado, fall 1993, *J. Geophys. Res.*, *102*, 6171–6186, doi:10.1029/96JD00693.

National Research Council (1991), *Rethinking the Ozone Problem in Urban and Regional Air Pollution*, Comm. on Tropospheric Ozone Form. and Measure., Natl. Acad. Press, Washington, D. C.

Paulot, F., J. D. Crounse, H. G. Kjaergaard, A. Kürten, J. M. St. Clair, J. H. Seinfeld, and P. O. Wennberg (2009a), Unexpected epoxide formation in the gas-phase photooxidation of isoprene, *Science*, *325*, 730–733, doi:10.1126/science.1172910.

Paulot, F., J. D. Crounse, H. G. Kjaergaard, J. H. Kroll, J. H. Seinfeld, and P. O. Wennberg (2009b), Isoprene photooxidation: New insights into the production of acids and organic nitrates, *Atmos. Chem. Phys.*, *9*, 1479–1501, doi:10.5194/acp-9-1479-2009.

Pöschl, U., R. von Kuhlmann, N. Poisson, and P. J. Crutzen (2000), Development and intercomparison of condensed isoprene oxidation mechanisms for global atmospheric modelling, *J. Atmos. Chem.*, *37*, 29–52, doi:10.1023/A:1006391009798.

Pugh, T. A. M., et al. (2010), Simulating atmospheric composition over a Southeast Asian tropical rainforest: Performance of a chemistry box model, *Atmos. Chem. Phys.*, *10*, 279–298, doi:10.5194/acp-10-279-2010.

Ren, X., W. H. Brune, C. A. Cantrell, G. D. Edwards, T. Shirley, A. R. Metcalf, and R. L. Lesher (2005), Hydroxyl and peroxy radical chemistry in a rural area of central Pennsylvania: Observation and model comparisons, *J. Atmos. Chem.*, *52*, 231–257, doi:10.1007/s10874-005-3651-7.

Ren, X., et al. (2006), Behavior of OH and HO_2 in the winter atmosphere in New York City, *Atmos. Environ.*, *40*, Suppl. 2, 252–263, doi:10.1016/j.atmosenv.2005.11.073.

Sander, R., A. Kerkweg, P. Jöckel, and J. Lelieveld (2005), Technical note: The new comprehensive atmospheric chemistry module MECCA, *Atmos. Chem. Phys.*, *5*, 445–450, doi:10.5194/acp-5-445-2005.

Saunders, S. M., M. E. Jenkin, R. G. Derwent, and M. J. Pilling (2003), Protocol for the development of the Master Chemical Mechanism, MCM V3: Tropospheric degradation of non-aromatic VOC, *Atmos. Chem. Phys.*, *3*, 161–180, doi:10.5194/acp-3-161-2003.

Schlosser, E., et al. (2009), Technical note: Formal blind intercomparison of OH measurements: Results from the international campaign HOxComp, *Atmos. Chem. Phys.*, *9*, 7923–7948, doi:10.5194/acp-9-7923-2009.

Sommariva, R., et al. (2006), OH and HO_2 chemistry during NAMBLEX: Roles of oxygenates, halogen oxides and heterogeneous uptake, *Atmos. Chem. Phys.*, *6*, 1135–1153, doi:10.5194/acp-6-1135-2006.

Stemmler, K., M. Ammann, C. Dondors, J. Kleffmann, and C. George (2006), Photosensitized reduction of nitrogen dioxide on humic acid as a source of nitrous acid, *Nature*, *440*, 195–198, doi:10.1038/nature04603.

Stockwell, W. R., F. Kirchner, M. Kuhn, and S. Seefeld (1997), A new mechanism for regional atmospheric chemistry modelling, *J. Geophys. Res.*, *102*(D22), 25,847–25,879, doi:10.1029/97JD00849.

Stone, D., et al. (2011), Isoprene oxidation mechanisms: Measurements and modelling of OH and HO2 over a South-East Asian tropical rainforest during the OP3 field campaign, *Atmos. Chem. Phys.*, *11*, 6749–6771, doi:10.5194/acp-11-6749-2011.

Su, H., Y. Cheng, R. Oswald, T. Behrendt, I. Trebs, F. X. Meixner, M. O. Andreae, P. Cheng, Y. Zhang, and U. Pöschl (2011), Soil nitrite as a source of atmospheric HONO and OH radicals, *Science*, *333*, 1616–1618, doi:10.1126/science.1207687.

Taraborrelli, D., M. G. Lawrence, T. M. Butler, R. Sander, and J. Lelieveld (2009), Mainz Isoprene Mechanism 2 (MIM2), An isoprene oxidation mechanism for regional and global atmospheric modelling, *Atmos. Chem. Phys.*, *9*, 2751–2777, doi:10.5194/acp-9-2751-2009.

von Kuhlmann, R., M. G. Lawrence, U. Pöschl, and P. J. Crutzen (2004), Sensitivities in global scale modelling of isoprene, *Atmos. Chem. Phys.*, *4*, 1–17, doi:10.5194/acp-4-1-2004.

Whalley, L. K., et al. (2011), Quantifying the magnitude of a missing hydroxyl radical source in a tropical rainforest, *Atmos. Chem. Phys.*, *11*, 7223–7233, doi:10.5194/acp-11-7223-2011.

Yoshino, A., A. Sadanagab, K. Watanabea, S. Katoa, Y. Miyakawaa, J. Matsumotoc, and Y. Kajiia (2006), Measurement of total OH reactivity by laser-induced pump and probe technique-comprehensive observations in the urban atmosphere of Tokyo, *Atmos. Environ.*, *40*, 7869–7881, doi:10.1016/j.atmosenv.2006.07.023.

Zhou, X., H. Gao, Y. He, G. Huang, S. B. Bertman, K. Civerolo, and J. Schwab (2003), Nitric acid photolysis on surfaces in low-NO_x environments: Significant atmospheric implications, *Geophys. Res. Lett.*, *30*(23), 2217, doi:10.1029/2003GL018620.

Zhou, X., et al. (2011), Nitric acid photolysis on forest canopy surface as a source for tropospheric nitrous acid, *Nat. Geosci.*, *4*, 440–443, doi:10.1038/ngeo1164.

H. Berresheim, School of Physics and Centre for Climate and Air Pollution Studies, National University of Ireland Galway, University Road, Galway, Ireland.

B. Bohn, T. Brauers, H.-P. Dorn, H. Fuchs, A. Hofzumahaus, F. Holland, F. Rohrer, R. Tillmann, A. Wahner, and R. Wegener, Institut für Energie- und Klimaforschung, Forschungzentrum Jülich, D-52425 Jülich, Germany.

Y. F. Elshorbany, H. Harder, D. Kubistin, J. Lelieveld, and M. Martinez, Atmospheric Chemistry Department, Max-Plank Institute für Chemie, J. Joachim-Becher-Weg 27, D-55128 Mainz, Germany. (yasin.elshorbany@mpic.de)

T. Elste, C. Plass-Dülmer, and G. Stange, Meteorologisches Observatorium, Deutscher Wetterdienst, Albin Schwaiger Weg 10, D-82383 Hohenpeissenberg, Germany.

Y. Kajii, Department of Applied Chemistry, Tokyo Metropolitan University, Tokyo 192-0397, Japan.

Y. Kanaya, Research Institute for Global Change, Japan Agency for Marine-Earth Science and Technology, 3173-25 Showa-machi, Kanazawa-ku, Yokohama, Kanagawa 236-0001, Japan.

J. Kleffmann, R. Kurtenbach, and P. Wiesen, Physikalische Chemie, FB C, Bergische Universität Wuppertal, Gaussstr. 20, D-42119 Wuppertal, Germany.

S. Nishida, Environmental Renewable Energy System Division, Graduate School of Engineering, Gifu University, 1-1, Yanagido, Gifu 501-1193, Japan.

U. Schurath, IMK-AAF, Karlsruhe Institute of Technology, Postfach 3640, Gebaeude 326, D-76021 Karlsruhe, Germany.

A. Yoshino, Environmental and Natural Resource Sciences, Tokyo University of Agriculture and Technology, 3-5-8 Saiwaicho, Fuchu, Tokyo 183-8509, Japan.